Polymer Chemistry

PAPER

View Article Online
View Journal | View Issue

Cite this: *Polym. Chem.*, 2015, **6**, 6998

Regioisomeric control of charge transport polarity for indigo-based polymers†

Chang Guo, Jesse Quinn, Bin Sun and Yuning Li*

In this work we report the opposite charge transport polarity observed for two regioisomeric polymer semiconductors. Previously, we observed n-type electron transport behaviour for a polymer semiconductor, **6,6′-PIDBDT**, which contains 6,6′-indigo units. Electron distributions in the lowest unoccupied molecular orbital (LUMO) and the highest occupied molecular orbital (HOMO) of indigo calculated by density functional theory (DFT) could explain the electron transport behaviour since electrons can be delocalized along the polymer backbone through the LUMO rather than the HOMO *via* the 6- and 6′-positions. Serendipitously, we found that the 5- and 5′-positions of indigo are occupied by electrons in the HOMO but empty in the LUMO, opposite to the 6- and 6′-positions. This suggests that **5,5′-PIDBDT** containing the 5,5′-indigo units, a regioisomer of **6,6′-PIDBDT**, may exhibit the opposite p-type charge transport behaviour. To prove our assumption, we synthesized **5,5′-PIDBDT** and found that this polymer indeed showed p-type semiconductor behaviour. Hence we demonstrated a novel approach to control the electron or hole charge transport polarity by simply varying the main chain regiochemical connections.

Received 29th May 2015,
Accepted 15th August 2015

DOI: 10.1039/c5py00821b

www.rsc.org/polymers

Introduction

Polymer semiconductors have been attracting tremendous attention due to their excellent solution processability, large area uniformity and mechanical robustness, making them suitable for printed electronics such as flexible displays, smart labels, photovoltaics, and sensors.[1–7] Organic thin film transistor (OTFT) based polymer semiconductors are fundamental elements for many printed electronics. In recent years, polymer semiconductors with good environmental stability and high charge carrier mobility in excess of 1 $cm^2\ V^{-1}\ s^{-1}$ have been reported.[4,7–13] Based on the type of charge carrier, polymer semiconductors can be classified into p-type and n-type, where positively charged holes are the carriers in the former, while negatively charged electrons are the carriers in the latter. The polarity (p-type or n-type) of a polymer semiconductor in an OTFT device is determined by the barriers of the frontier orbital energy levels, *i.e.*, the highest occupied molecular orbital (HOMO) and the lowest unoccupied molecular orbital (LUMO), with respect to the Fermi energy level (E_F) of the source electrode material.[8,14,15] For a p-type semiconductor, a higher HOMO is preferred for hole injection and transport, while for an n-type polymer, a lower LUMO is desirable for electron injection and transport. Additionally, the HOMO and LUMO levels need to be sufficiently low for realization of hole or electron transport in the presence of water, hydroxyl groups, or oxygen. Experimentally, a HOMO level below ~−5.0 eV[3,16,17] and a LUMO level below ~−3.7 eV[16,18–20] are required for stable hole and electron transport, respectively. So far, the most widely used strategy to control the polarity of polymer semiconductors is to tune the HOMO and LUMO energy levels by using various electron donor and acceptor building blocks. Alternatively, the polarity can be changed by varying the work function (or Fermi energy) of the source conductor material through surface modification.[21–23]

In this study, we report a new approach to changing the charge transport polarity by choosing regioisomerically different building blocks in the polymer semiconductors. Two indigo-based polymers with the exactly same chemical compositions but different regioisomeric connections were found to show opposite polarity.

Results and discussion

Previously we used a naturally occurring indigo dye, Tyrian purple (6,6′-dibromoindigo), as a starting material to construct polymer semiconductors, **PIDBT**[24] and **6,6′-PIDBDT**[25] (Fig. 1), as channel materials for OTFTs. N-type electron transport performance was observed for these polymers. We carried out

Department of Chemical Engineering and Waterloo Institute for nanotechnology (WIN), University of Waterloo, 200 University Ave West ON, Waterloo, Canada N2L 3G1. E-mail: yuning.li@uwaterloo.ca; Fax: +1-519-888-4347; Tel: +1 1-519-888-4567 ext.31105

†Electronic supplementary information (ESI) available: Details of computer simulations, NMR spectra of **1**, **3** and **5,5′-PIDBDT**, XRD and AFM data. See DOI: 10.1039/c5py00821b

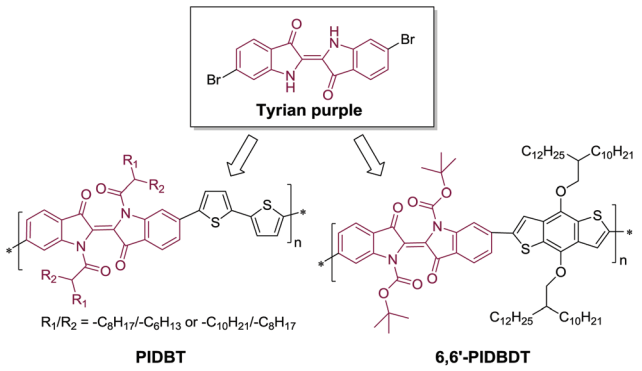

Fig. 1 Chemical structures of Tyrian purple (6,6′-dibromoindigo) and polymers, **PIDBT**[24] and **6,6′-PIDBDT**,[25] prepared from Tyrian purple.

density functional theory (DFT) calculations on indigo (ID) and found that electrons are distributed on the 6- and 6′-positions of ID in the LUMO but not in the HOMO (Fig. 2). Therefore when the ID unit is connected with another conjugated comonomer unit through the 6- and 6′-positions, the resulting polymer would allow extended π-electron delocalization in the LUMO along the polymer backbone but prohibit the π-electron delocalization in the HOMO. This might explain the n-type electron transport behaviour of **PIDBT** and **6,6′-PIDBDT**, which have ID units connected through the 6- and 6′-positions. Interestingly, we noticed that electrons are distributed in the HOMO but not in the LUMO at the 5- and 5′-positions, which is opposite to the case of the 6- and 6′-positions. Accordingly, we expected that polymers containing ID units connected through the 5- and 5′-positions might exhibit p-type hole transport behaviour instead of n-type electron transport behaviour.

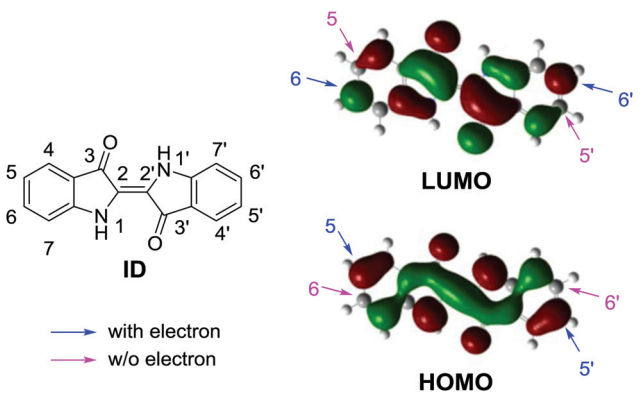

Fig. 2 Indigo (ID) and its wave functions of the highest occupied molecular orbital (HOMO) and the lowest unoccupied molecular orbital (LUMO) obtained by density functional theory (DFT) calculations.

6,6′-PIDBDT, which has a thermally labile *tert*-butoxy carbonyl (*t*-Boc) group, was previously found to be able to retrieve the highly coplanar geometry of the ID units after thermal removal of the *t*-Boc groups, leading to much higher mobility than that of **PIDBT**. Therefore in this study we designed its regioisomer, **5,5′-PIDBDT** (Scheme 1), where each *t*-Boc-substituted ID unit is connected through the 5- and 5′-positions with two neighbouring benzo[1,2-*b*:4,5-*b*′]dithiophene (BDT) units. By using DFT calculations with Gaussian 09W[26,27] at the B3LYP/6-31G(d) level, we simulated two dimer compounds, 5,5′-ID-BDT-ID-BDT and 6,6′-ID-BDT-ID-BDT of **5,5′-PIDBDT** and **6,6′-PIDBDT** after removal of the *t*-Boc groups, respectively (Fig. 3). Similar to the HOMO and LUMO wave functions of ID (Fig. 2), in both dimers, the 5- and 5′-positions of the ID unit are occupied by electrons in the HOMO but empty in the LUMO. Conversely the 6- and 6′-positions of the ID unit are empty in the HOMO but occupied in the LUMO. The calculated HOMO and LUMO levels are −5.03 eV and −2.96 eV, respectively, for 5,5′-ID-BDT-ID-BDT, and −5.30 eV and −2.96 eV, respectively, for 6,6′-ID-BDT-ID-BDT, indicating that the HOMO level of **5,5′-PIDBDT** is raised compared to **6,6′-PIDBDT** due to the more effective hybridization of π-electrons in the HOMO along the polymer chain of the former polymer.

5,5′-PIDBDT was synthesized according to Scheme 1. Compound **1** was readily prepared in 76% yield by using a literature method.[28] Compound **2** (5,5′-dibromoindigo) was then synthesized in 75% yield by stirring **1** in acetone in the presence of aq. NaOH at room temperature. Substitution of **2** with the *t*-Boc groups using di-*tert*-butyl 3,3′-dioxo-[2,2′-biindolinylidene]-1,1′-dicarboxylate yielded compound **3** (83%). Finally polymer **5,5′-PIDBDT** was obtained by the Stille coupling polymerization between **3** and (4,8-bis((2-decyltetradecyl)oxy)-benzo[1,2-*b*:4,5-*b*′]dithiophene-2,6-diyl)bis(trimethylstannane)

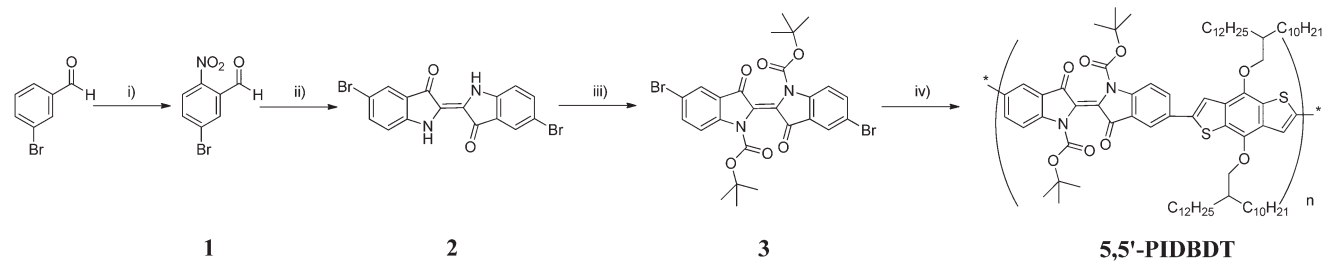

Scheme 1 Synthetic route to **5,5′-PIDBDT**. Reagents and conditions: (i) HNO_3/H_2SO_4/0 °C to r.t.; (ii) NaOH/acetone/r.t.; (iii) 4-dimethylaminopyridine/di-*tert*-butyldicarbonate/DMF/0 °C to r.t.; (iv) (4,8-bis((2-decyltetradecyl)oxy)benzo[1,2-*b*:4,5-*b*′]dithiophene-2,6-diyl)bis(trimethylstannane)/Pd_2dba_3/P(*o*-tolyl)$_3$/110 °C.

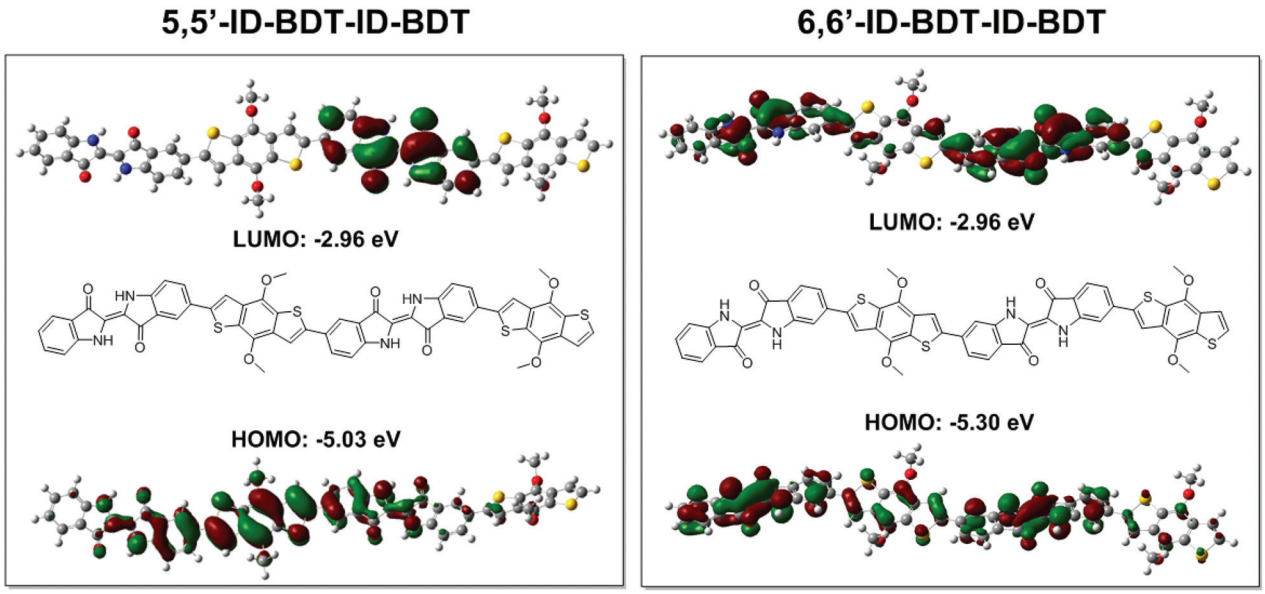

Fig. 3 HOMO and LUMO electron distributions and energy levels of 5,5′-ID-BDT-ID-BDT and 6,6′-ID-BDT-ID-BDT obtained by density functional theory (DFT) calculations.

with tris(dibenzylideneacetone)dipalladium (Pd_2dba_3)/tri-(*o*-tolyl)phosphine ($P(o\text{-tolyl})_3$) as a catalyst in chlorobenzene at 110 °C for 60 h. The obtained crude polymer was subjected to consecutive Soxhlet extraction with acetone, hexane, and chloroform. The yield of the polymer extracted with chloroform is 39%. The molecular weight of **5,5′-PIDBDT** was determined by gel-permeation chromatography (GPC) with chlorobenzene as an eluent and polystyrene as a standard at a column temperature of 40 °C. The number average molecular weight (M_n) of **5,5′-PIDBDT** (extracted with chloroform) is 32.6 kDa with a polydispersity index (PDI) of 2.53.

The purpose of using the thermocleavable *t*-Boc groups in **5,5′-PIDBDT** is to retrieve the highly coplanar geometry of the ID units for improving the intramolecular charge transport by thermal annealing.[25] Thermogravimetric analysis (TGA) showed that **5,5′-PIDBDT** started to lose weight at ~170 °C and reached a flat region with a weight loss of ~15% at ~240 °C (Fig. 4). The weight loss agrees with the calculated amount of the *t*-Boc groups (~15%) in the polymer, indicating a complete removal of the *t*-Boc groups in this region. The second abrupt weight loss started at ~280 °C is caused by further decomposition of the polymer. The thermal decomposition behaviour of **5,5′-PIDBDT** is very similar to that of its regioisomer, **6,6′-PIDBDT**.[25]

Compounds **2** and **3** were dissolved in dilute 1,1,2,2-tetrachloroethane (TCE) to obtain their UV-vis absorption spectra (Fig. 5a). Compound **2** showed a wavelength of the maximum absorption (λ_{max}) at 621 nm, while compound **3** showed a ~60 nm blue shift in λ_{max} due to the twisting of this molecule caused by the *t*-Boc groups. A dilute solution of **5,5′-PIDBDT** in 1,2,4-trichlorobenzene showed a λ_{max} at ~630 nm (Fig. 5b). After being heated at 200 °C for 1 h and cooled down to room

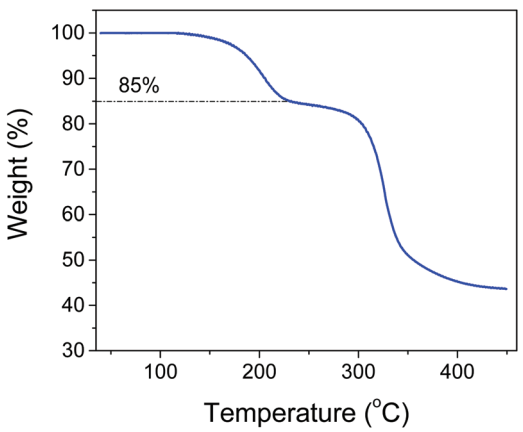

Fig. 4 TGA curves of **5,5′-PIDBDT** at a heating rate of 10 °C min^{-1} under nitrogen.

temperature, the measured λ_{max} red shifted to ~665 nm, indicating the more coplanar geometry of the polymer main chains after thermal removal of the *t*-Boc groups. Fig. 5c shows the spectral changes of the **5,5′-PIDBDT** polymer thin films on glass substrates after annealing at 200 °C for 1 h. Compared to the non-annealed film, the λ_{max} of the 200 °C-annealed film red shifted from 642 nm to 669 nm, similar to the phenomenon observed for the heated solution. Cyclic voltammetry (CV) was used to determine the energy levels of **5,5′-PIDBDT** thin films spin coated on conductive indium tin oxide (ITO) substrates (Fig. 6). The non-annealed polymer thin film has HOMO and LUMO levels of −5.6 eV and −3.6 eV, respectively, with ferrocene as the reference (−4.8 eV).[29] After annealing at 200 °C for 1 h, the LUMO level of the polymer film remained

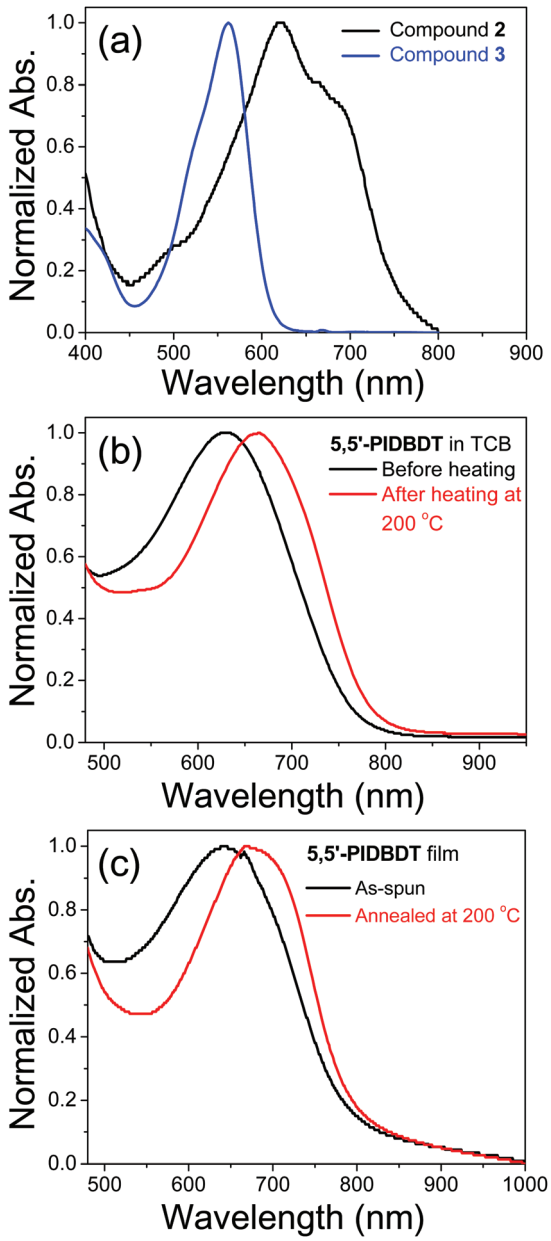

Fig. 5 UV-vis absorption spectra of (a) compounds **2** and **3** in TCE solutions, (b) a solution of **5,5′-PIDBDT** in 1,2,4-trichlorobenzene (TCB) before and after heating at 200 °C for 1 h, and (c) a **5,5′-PIDBDT** film spin coated on a glass substrate before (as-spun) and after annealing at 200 °C for 1 h.

at ~−3.6 eV, while the HOMO level increased to −5.3 eV. In comparison with the 200 °C-annealed **6,6′-PIDBDT**, which showed HOMO and LUMO levels of −5.8 eV and −4.2 eV,[25] the 200 °C-annealed **5,5′-PIDBDT** has significantly higher HOMO and LUMO levels, which would favour hole transport over electron transport.

A top-gate, bottom-contact OTFT device configuration was used to evaluate **5,5′-PIDBDT** as a channel semiconductor. A solution of **5,5′-PIDBDT** (10 mg mL^{-1}) in a mixture of chloroform/1,2-dichlorobenzene (v/v = 9/1) was spin coated on an

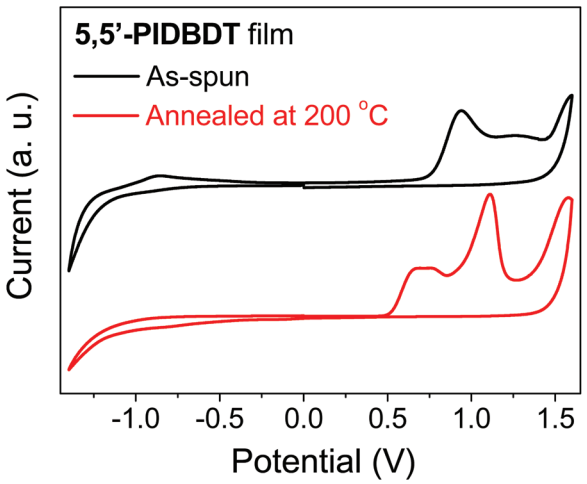

Fig. 6 Cyclic voltammograms of an as-spun and 200 °C-annealed **5,5′-PIDBDT** thin film measured in anhydrous CH_3CN solution using Bu_4NPF_6 as the electrolyte.

n-doped Si/SiO_2 wafer patterned with gold source and drain electrode pairs to form a thin film (~40 nm). After thermal annealing at 100 °C, 150 °C, 200 °C or 250 °C for 1 h on a hot plate, a CYTOP layer (~570 nm) was spin coated to form the gate dielectric. Finally an Al layer (~70 nm) was thermally evaporated as the gate electrode. The devices were characterized in air in the absence of light. While the 100 °C- and 150 °C-annealed polymer films showed no field effect behaviour, the devices annealed at 200 °C exhibited typical p-type hole transport characteristics with mobility as high as 2.5 × 10^{-4} cm^2 V^{-1} s^{-1} (and a current on-to-off ratio of ~10^3) (Fig. 7). The appearance of field effect performance for the films annealed at 200 °C is due to the backbone coplanarization by thermal removal of the *t*-Boc groups, which allowed extended π-electron delocalization along the polymer main chains to facilitate intramolecular charge transport. A similar phenomenon was observed for **6,6′-PIDBDT**,[25] which showed the charge transport performance only after the *t*-Boc groups were

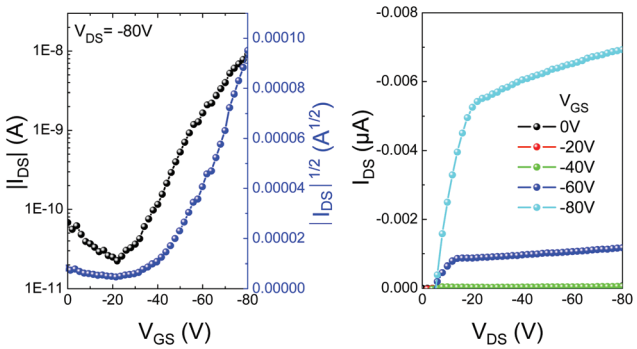

Fig. 7 Transfer (left) and output curves (right) of an OTFT device with a **5,5′-PIDBDT** thin film annealed at 200 °C for 1 h. Device dimensions: channel width (*W*) = 1 mm; channel length (*L*) = 30 μm.

removed at 200 °C. However, **6,6′-PIDBDT** showed the opposite n-type electron transport performance. The results fully supported our prediction on the charge transport polarity for **5,5′-PIDBDT** based on DFT calculations. The mobility of **5,5′-PIDBDT** is lower compared to that of **6,6′-PIDBDT**, which might be due to its poor crystallinity verified by the X-ray diffractometry (XRD) measurement (see the ESI†). The devices annealed at 250 °C did not show field effect performance, which might be due to the decomposition of the polymer.

Experimental

Materials and characterization

All chemical reagents were purchased from commercial sources and used without further purification. 5-Bromo-2-nitrobenzaldehyde (**1**)[28] and (4,8-bis((2-decyltetradecyl)oxy)-benzo[1,2-*b*:4,5-*b*′]dithiophene-2,6-diyl)bis(trimethylstannane)[30] were synthesized by following the reported procedures. NMR spectra were obtained on a Bruker DPX 300 MHz spectrometer using tetramethylsilane (TMS, 0 ppm) as a reference. A Thermo Scientific GENESYS[20] Spectrophotometer was used to collect UV-Vis spectra. Cyclic voltammetry (CV) experiments were carried out on an electrochemical analyser CHI600E, using an Ag/AgCl reference electrode, a Pt wire counter electrode, and a Pt foil working electrode in 0.1 M tetrabutylammonium hexafluorophosphate in dry acetonitrile under nitrogen. Ferrocene was used as a reference, which has the highest occupied molecular orbital (HOMO) energy level of −4.8 eV.[29] Gel-permeation chromatography (GPC) measurements were performed on a Waters SEC with chlorobenzene as an eluent at 40 °C. A TGA Q500 (TA Instruments) system was used to conduct the thermogravimetric analysis (TGA) under nitrogen at a heating rate of 10 °C min^{-1}. A Bruker D8 Advance powder diffractometer with standard Bragg–Brentano geometry using Cu Kα_1 radiation (λ = 1.5406 Å) was used to record the XRD diagrams of polymer thin films (~70 nm). The atomic force microscopy (AFM) images of polymer thin films were recorded by using a Dimension 3100 Scanning Probe Microscope.

OTFT fabrication and characterization

A top-gate, bottom-contact OTFT structure was adopted for evaluating **5,5′-PIDBDT** with a heavily n-doped Si/SiO_2 wafer as the substrate. The gold source/drain electrode pairs were deposited using conventional photolithography to obtain the defined device dimensions with a channel length (L) of 30 μm and a channel width (W) of 1 mm. The substrate was cleaned using an ultrasonic bath with DI water, and rinsed with acetone and isopropanol. The polymer films with thickness ~40 nm were deposited on the substrate by spin-coating a polymer solution (10 mg mL^{-1}) in chloroform/1,2-dichlorobenzene (volume ratio = 9 : 1) at 3000 rpm for 60 s subsequently annealed at 100, 150, 200 and 250 °C for 1 h. A CYTOP (an amorphous fluoropolymer of AGC Chemicals) layer was then deposited by spin coating a CYTOP solution as the gate dielectric, and then dried at 100 °C on a hotplate for 30 min before depositing the Al gate electrode (~70 nm) by using a thermal evaporator. All devices were characterized in air in the absence of light using an Agilent 4155C Semiconductor Analyser. Carrier mobility was calculated in the saturation regime according to the equation below:

$$I_D = \left(\frac{WC_i}{2L}\right)\mu(V_G - V_T)2$$

where I_D is the drain current, μ is the charge carrier mobility, C_i is the capacitance per unit area of the insulator determined from a metal–insulator–metal structure (CYTOP, 570 nm, C_i = 3.2 nF cm^{-2}), V_G is the gate voltage, respectively.

Synthesis

5-Bromo-2-nitrobenzaldehyde (1).[28] At 0 °C, 3-bromobenzaldehyde (4.12 g, 22.3 mmol) was added in small portions into a mixture of HNO_3 (60–70% solution in H_2O, 5 mL) and H_2SO_4 (96%, 10 mL) over a period of 30 min. The resulting yellow suspension was then stirred at room temperature for another 45 min. The mixture was slowly poured into saturated $NaHCO_3$ solution (60 mL) maintained at 0 °C with stirring and then extracted with ethyl acetate. The combined organic layers were washed with a saturated $NaHCO_3$ solution until the pH of the aqueous phase was ~8–9. The organic phase was dried over Na_2SO_4 and filtered. After evaporation of the solvent, the crude product was purified by column chromatography (hexane/DCM = 2 : 1) to give a dark-orange solid. Yield: 3.90 g (76%). ^{1}H NMR (300 MHz, $CDCl_3$) δ 10.42 (s, 1H), 8.07 (d, J = 2.2 Hz, 1H), 8.03 (d, J = 8.6 Hz, 1H), 7.88 (dd, J = 8.7, 2.2 Hz, 1H).

5,5′-Dibromo-[2,2′-biindolinylidene]-3,3′-dione (2). Compound **2** was synthesized following a similar procedure for the synthesis of 6,6′-dibromo-[2,2′-biindolinylidene]-3,3′-dione.[25] Compound **1** (1 g, 4.4 mmol) was dissolved in acetone (45 mL), followed by slow addition of water (50 mL). Then a 2 N aqueous NaOH solution was added dropwise at room temperature to adjust the pH to 10. The mixture was stirred overnight at room temperature and filtered. The solid was washed with excess acetone and de-ionized (DI) water, and dried *in vacuo* to give a blue powder. Yield: 0.69 g (75%). This product has poor solubility in organic solvents and was used for the next step reaction without further purification. Synthesis of compound **2** was reported previously using a different procedure.[31]

Di-*tert*-butyl 5,5′-dibromo-3,3′-dioxo-[2,2′-biindolinylidene]-1,1′-dicarboxylate (3). Compound **3** was synthesized following a similar procedure for the synthesis of di-*tert*-butyl 6,6′-dibromo-3,3′-dioxo-[2,2′-biindolinylidene]-1,1′-dicarboxylate.[25] To a suspension of compound **2** (0.336 g, 0.8 mmol) and 4-dimethylaminopyridine (57 mg, 0.46 mmol) in *N*,*N*-dimethylformamide (DMF) (3 mL) was added di-*tert*-butyldicarbonate (0.922 g, 4.22 mmol) in two portions at 0 °C. Then the mixture was stirred for 20 h at room temperature, during which time the color of the suspension changed from dark red to bright red. The product was isolated by filtration and the residue was washed with DMF and de-ionized (DI) water, and dried. Recrys-

tallization of the solid from a mixture of chloroform/isopropanol gave a dark red powder. Yield: 0.265 g (53%). ^{1}H NMR (300 MHz, $CDCl_3$) δ 7.92 (d, J = 8.8 Hz, 2H), 7.87 (d, J = 2.0 Hz, 2H), 7.70 (dd, J_1 = 8.8 Hz, J_2 = 2.0 Hz, 2H), 1.60 (s, 18H).

HRMS $(M + H)^+$ calc. for $C_{26}H_{23}Br_2N_2O_6^+$: 618.9902; found: 619.0067.

Synthesis of compound **3** was reported previously using a different procedure.[32]

5,5′-PIDBDT. To a 25 mL dry Schlenk flask was added **3** (0.0557 g, 0.09 mmol), (4,8-bis((2-decyltetradecyl)oxy)benzo[1,2-*b*:4,5-*b*′]dithiophene-2,6-diyl)bis(trimethylstannane) (0.110 g, 0.09 mmol) and tri(*o*-tolyl)phosphine (P(*o*-tolyl)$_3$) (2 mg, 0.007 mmol). After degassing and refilling argon 3 times, anhydrous chlorobenzene (3 mL) and tris(dibenzylideneacetone)dipalladium (Pd_2dba_3) (1.6 mg, 0.002 mmol) were added under an argon atmosphere. The mixture was stirred for 60 h at 110 °C under argon before cooling to room temperature. After bromobenzene (0.5 mL) was added, the mixture was heated to 110 °C again and stirred for an additional 2 h. The cooled mixture was poured into methanol, and the precipitate was collected by filtration and subjected to Soxhlet extraction sequentially with acetone, hexane and chloroform. Yield of the chloroform extracted fraction: 47 mg (39%). GPC data: number average molecular weight (M_n) = 32.6 kDa; polydispersity index (PDI) = 2.53.

Conclusions

The HOMO and LUMO wave functions of the indigo (ID) unit obtained by DFT calculations showed that electrons were differently (oppositely) distributed on the 6,6′-positions and the 5,5′-positions. While the simulation results could explain the n-type electron transport behaviour of **6,6′-PIDBDT** containing 6,6′-ID units, they also led us to predict that the regioisomeric polymer **5,5′-PIDBDT**, which contains 5,5′-ID units, would favour p-type hole transport performance. To prove our assumption, we synthesized **5,5′-PIDBDT**, which was found to have higher HOMO and LUMO energy levels compared to **6,6′-PIDBDT**, after thermal removal of the *t*-Boc groups. As expected, the annealed **5,5′-PIDBDT** showed p-type hole transport behaviour in OTFT devices, which is opposite to that of its regioisomer **6,6′-PIDBDT**. This work inspired by a serendipitous finding demonstrated a new way to predict and control the polarity of a polymer semiconductor by examining the HOMO and LUMO wave functions using computer simulations.

Acknowledgements

The authors thank the NSERC Discovery Grants (#402566-2011) from the federal government of Canada for financial support of this research.

Notes and references

1 H. Klauk, *Chem. Soc. Rev.*, 2010, **39**, 2643–2666.
2 A. C. Arias, J. D. MacKenzie, I. McCulloch, J. Rivnay and A. Salleo, *Chem. Rev.*, 2010, **110**, 3–24.
3 A. Facchetti, *Chem. Mater.*, 2011, **23**, 733–758.
4 C. Guo, W. Hong, H. Aziz and Y. Li, *Rev. Adv. Sci. Eng.*, 2012, **1**, 200–224.
5 P. Lin and F. Yan, *Adv. Mater.*, 2012, **24**, 34–51.
6 A. Facchetti, *Mater. Today*, 2013, **16**, 123–132.
7 Y. He, W. Hong and Y. Li, *J. Mater. Chem. C*, 2014, **2**, 8651–8661.
8 Y. Li, P. Sonar, L. Murphy and W. Hong, *Energy Environ. Sci.*, 2013, **6**, 1684–1710.
9 H. Sirringhaus, *Adv. Mater.*, 2014, **26**, 1319–1335.
10 B. Sun, W. Hong, Z. Yan, H. Aziz and Y. Li, *Adv. Mater.*, 2014, **26**, 2636–2642.
11 C. Luo, A. K. K. Kyaw, L. A. Perez, S. Patel, M. Wang, B. Grimm, G. C. Bazan, E. J. Kramer and A. J. Heeger, *Nano Lett.*, 2014, **14**, 2764–2771.
12 X. Zhou, N. Ai, Z.-H. Guo, F.-D. Zhuang, Y.-S. Jiang, J.-Y. Wang and J. Pei, *Chem. Mater.*, 2015, **27**, 1815–1820.
13 B. Fu, C.-Y. Wang, B. D. Rose, Y. Jiang, M. Chang, P.-H. Chu, Z. Yuan, C. Fuentes-Hernandez, B. Kippelen, J.-L. Brédas, D. M. Collard and E. Reichmanis, *Chem. Mater.*, 2015, **27**, 2928–2937.
14 J. Cornil, D. Beljonne, J.-P. Calbert and J.-L. Brédas, *Adv. Mater.*, 2001, **13**, 1053–1067.
15 J. L. Brédas, J. P. Calbert, D. A. da Silva Filho and J. Cornil, *Proc. Natl. Acad. Sci. U. S. A.*, 2002, **99**, 5804–5809.
16 D. M. de Leeuw, M. M. J. Simenon, A. R. Brown and R. E. F. Einerhand, *Synth. Met.*, 1997, **87**, 53–59.
17 B. S. Ong, Y. Wu, P. Liu and S. Gardner, *J. Am. Chem. Soc.*, 2004, **126**, 3378–3379.
18 H. Yan, Z. Chen, Y. Zheng, C. Newman, J. R. Quinn, F. Dotz, M. Kastler and A. Facchetti, *Nature*, 2009, **457**, 679–686.
19 Z. Yan, B. Sun and Y. Li, *Chem. Commun.*, 2013, **49**, 3790–3792.
20 L. Wang, X. Zhang, H. Tian, Y. Lu, Y. Geng and F. Wang, *Chem. Commun.*, 2013, **49**, 11272–11274.
21 X. Cheng, Y.-Y. Noh, J. Wang, M. Tello, J. Frisch, R.-P. Blum, A. Vollmer, J. P. Rabe, N. Koch and H. Sirringhaus, *Adv. Funct. Mater.*, 2009, **19**, 2407–2415.
22 B. Sun, W. Hong, E. Thibau, H. Aziz, Z.-H. Lu and Y. Li, *Org. Electron.*, 2014, **15**, 3787–3794.
23 B. Sun, W. Hong, H. Aziz and Y. Li, *Polym. Chem.*, 2015, **6**, 938–945.
24 C. Guo, B. Sun, J. Quinn, Z. Yan and Y. Li, *J. Mater. Chem. C*, 2014, **2**, 4289–4296.
25 C. Guo, J. Quinn, B. Sun and Y. Li, *J. Mater. Chem. C*, 2015, **3**, 5226–5232.
26 M. J. Frisch, *Gaussian 09 Programmer's Reference*, Gaussian, 2009.
27 M. J. Frisch, *et al.*, *Gaussian 09*, 2009; See the ESI† for the full citation.
28 M. Peters, M. Trobe, H. Tan, R. Kleineweischede and R. Breinbauer, *Chem. – Eur. J.*, 2013, **19**, 2442–2449.

29 B. W. D'Andrade, S. Datta, S. R. Forrest, P. Djurovich, E. Polikarpov and M. E. Thompson, *Org. Electron.*, 2005, **6**, 11–20.
30 Q. Shi, H. Fan, Y. Liu, J. Chen, L. Ma, W. Hu, Z. Shuai, Y. Li and X. Zhan, *Macromolecules*, 2011, **44**, 4230–4240.
31 P. Friedländer, S. Bruckner and G. Deutsch, *Justus Liebigs Ann. Chem.*, 1912, **388**, 23–49.
32 E. D. Glowacki, G. Voss, K. Demirak, M. Havlicek, N. Sunger, A. C. Okur, U. Monkowius, J. Gasiorowski, L. Leonat and N. S. Sariciftci, *Chem. Commun.*, 2013, **49**, 6063–6065.